Chapter 6
Heat and Mass Transfer of a Rotating Disk for Large Prandtl and Schmidt Numbers

6.1 Laminar Flow

Convective heat and mass transfer over a single disk rotating in fluid with high Prandtl or Schmidt numbers can be found in many practical and research applications. For instance, in electrochemistry, where the Schmidt numbers are several orders of magnitude larger than unity, rotating disk electrode is involved in measurements of the convective diffusion coefficient [1–14]. Another example is naphthalene sublimation technique often used to measure mass transfer coefficients α_m [15–29].

The differential Eq. (1.28) of convective diffusion, including the time-averaged fluctuating components, is analogous to the energy Eq. (2.5), provided that the temperature T and the thermal diffusivity a are replaced by the concentration C and the diffusion coefficient D_m, respectively. The Navier–Stokes and continuity equations hold, if constant fluid properties are assumed.

If the Schmidt number Sc replaces the Prandtl number, and the nondimensional function θ is written as

$$\theta = (C - C_\infty)/(C_w - C_\infty), \tag{6.1}$$

then the self-similar Eqs. (2.32)–(2.36) for steady-state axisymmetric laminar flow become valid for convective mass transfer.

Surface concentration on the disk does not vary; thus $C_w = \text{const}$. Therefore, rewritten convective diffusion Eq. (2.36) reduces to

$$\theta'' - ScH\theta' = 0. \tag{6.2}$$

The following equations (analogous to Eq. (3.4)) can be used for estimation of the Sherwood number

I.V. Shevchuk, *Modelling of Convective Heat and Mass Transfer in Rotating Flows*, Mathematical Engineering, DOI 10.1007/978-3-319-20961-6_6

$$Sh = K_1 Re_{\omega}^{n_R}, \quad Sh_{av} = K_2 Re_{\varphi}^{n_R}. \tag{6.3}$$

The constants K_1 and K_2 in Eq. (6.3) are affected by the boundary conditions, flow type (laminar, transitional, or turbulent) and the Schmidt numbers. The exponent n_R is affected by the flow type, whereas $K_1 = K_2$ and $n_R = 1/2$ in a laminar flow regime.

Thus, the aforementioned analogy between convective heat and mass transfer, enables the use of theoretical solutions or empirical experimental equations simply via replacing C, Sc and Sh with of T, Pr and Nu (or vice versa), accordingly.

For laminar flow, Eqs. (2.32)–(2.36) for $Pr > 1$ and $Sc > 1$ at $N = 0$ and $\beta = 0$ were solved numerically using Mathcad [30]. Table 6.1 shows that the calculated coefficient K_1 is increasing with growing Pr or Sc numbers.

For the same Prandtl number, the constant K_1 is an increasing function of the exponent n_*: the value of K_1 at $Pr = 0.71$, 2.0 and 10^6 becomes 3.3, 2.73 and 2.2 times larger, respectively, if the constant n_* changes from −1 to 3. Thus, at increased Prandtl numbers, the influence of the exponent n_* on the constant K_1 gets less pronounced.

The approximate Eq. (3.6) for the coefficient K_1 for the boundary condition (2.30), $Pr \geq 1$ and nonzero values n_* was derived by Dorfman [31]. Values of K_1 by Eq. (3.6) surpass the exact solution. Equation (3.6) deviates from the exact solution at $n_* \leq 0$ by 16–40 % even for $Pr = 1$. For $n_* = 0$ and $Pr = 1$–3, this deviation reaches 10–11 %. For larger exponents n_* and $Pr = 1$–3, the deviation of

Table 6.1 Values of the constant K_1, exact solution of Eqs. (2.32)–(2.36) for $Pr > 1$ [30]

Pr (Sc)	$n_* = -2$	$n_* = -1.5$	$n_* = -1$	$n_* = -0.5$	$n_* = 0$	$n_* = 1$	$n_* = 2$	$n_* = 3$	$n_* = 4$
1.0	0.0	0.1305	0.2352	0.3221	0.3963	0.5180	0.6159	0.6982	0.7693
1.5	0.0	0.1682	0.2979	0.4028	0.4906	0.6324	0.7450	0.8389	0.9199
2.0	0.0	0.1989	0.3482	0.4669	0.5653	0.7226	0.8466	0.9498	1.0386
2.28	0.0	0.2140	0.3728	0.4982	0.6016	0.7663	0.8960	1.0036	1.0963
2.5	0.0	0.2251	0.3907	0.5209	0.6280	0.7982	0.9319	1.0428	1.1383
3.0	0.0	0.2480	0.4279	0.5680	0.6826	0.8640	1.0061	1.1238	1.2251
5.0	0.0	0.3206	0.5445	0.7153	0.8533	1.0697	1.2382	1.3774	1.4971
10.0	0.0	0.4410	0.7368	0.9577	1.1341	1.4083	1.6206	1.7957	1.9460
15.0	0.0	0.5254	0.8710	1.1268	1.3300	1.6446	1.8877	2.0880	2.2599
20.0	0.0	0.5924	0.9776	1.2610	1.4855	1.8323	2.0999	2.3203	2.5095
50	0.0	0.8536	1.3925	1.7835	2.0909	2.5635	2.9269	3.2260	3.4825
100	0.0	1.1108	1.8009	2.2979	2.6871	3.2840	3.7422	4.1190	4.4421
500	0.0	1.9943	3.2033	4.0644	4.7351	5.7596	6.5442	7.1888	7.7413
1000	0.0	2.5467	4.0802	5.1691	6.0162	7.3083	8.2972	9.1096	9.8057
10^4	0.0	5.6363	8.9846	11.348	13.181	15.971	18.104	19.855	21.356
10^5	0.0	12.291	19.548	24.657	28.613	34.632	39.230	43.003	46.236
10^6	0.0	26.626	42.304	53.328	61.860	74.834	84.742	92.873	99.838

Eq. (3.6) from the exact solution is smaller (1–6 %). However, at $Pr \rightarrow \infty$, the inaccuracy of Eq. (3.6) abruptly increases [30].

The functional dependence of the constant K_1 on the Schmidt (or Prandtl) number according to Dorfman's Eq. (3.6) and the exact solution for $n_* = 0$ (T_w = const. or C_w = const.) is depicted in Fig. 6.1. The inaccuracies of Eq. (3.6) make it unusable already for Sc = 1–3.

Equations (3.7) and (3.8) can be rewritten for mass transfer for $Sc = 0$–∞, respectively

$$K_1 = 0.6109Sc/(0.5301 + 0.3996Sc^{1/2} + Sc)^{2/3}, \tag{6.4}$$

$$K_1 = 0.6Sc/(0.56 + 0.26Sc^{1/2} + Sc)^{2/3}. \tag{6.5}$$

Equations (6.4) and (6.5) result nearly in the same values. Maximal deviation of them from the exact solution is 4 and 5 %, respectively, for Sc = 5–20 (Fig. 6.1). For higher Schmidt numbers, inaccuracies of Eqs. (6.4) and (6.5) tend to zero (Table 6.2).

Another expression was derived in the work [13]

$$K_1 = 0.621Sc/(1 + 0.298Sc^{-1/3} + 0.14514Sc^{-2/3}). \tag{6.6}$$

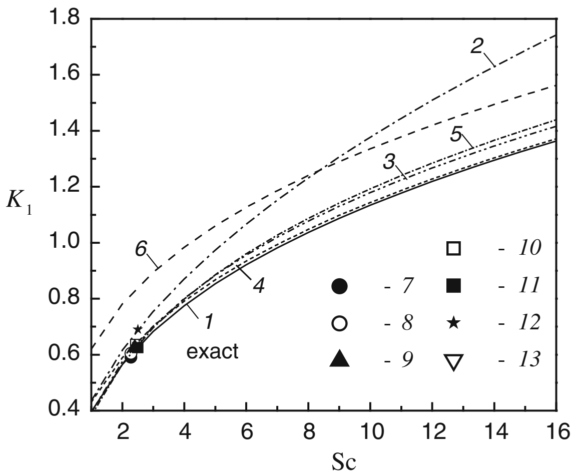

Fig. 6.1 Constant K_1 in Eq. (6.3), laminar flow at C_w = const. [30]. *1*—Exact solution; *2*—Eq. (3.6) for $n_* = 0$; *3*—Eqs. (6.4) and (6.5); *4*—Eq. (6.6); *5*—Eq. (6.7); *6*—Eq. (6.8). Experiments: *7*—$K_1 = 0.59$, $Sc = 2.28$ [15]; *8*—$K_1 = 0.604$, $Sc = 2.28$ [17]; *9*—$K_1 = 0.625$, $Sc = 2.4$ [20, 21, 26]; *10*—$K_1 = 0.636$, $Sc = 2.44$ [19]; *11*—$K_1 = 0.625$, $Sc = 2.5$ [25]; *12*—$K_1 = 0.69$, $Sc = 2.5$ [24]; *13*—$K_1 = 0.628$, $Sc = 2.5$ [22]

Table 6.2 Constant K_1 by Eqs. (6.4)–(6.8), a rotating disk for C_w = const. or T_w = const. [30]

Pr (*Sc*)	Exact	(6.4) [33]	(6.5) [34]	(6.6) [13]	(6.7) [2]	(6.8) [11]
1.0	0.3963	0.3941	0.4025	0.4303	0.3827	0.62
2.0	0.5653	0.5753	0.5864	0.5892	0.5664	0.7812
2.28	0.6016	0.6144	0.6257	0.6238	0.6065	0.816
2.5	0.6280	0.6430	0.6543	0.6491	0.6358	0.8415
5.0	0.8533	0.8839	0.8946	0.8676	0.8855	1.0602
20.0	1.4855	1.5414	1.5414	1.4924	1.5688	1.6829
50	2.0909	2.1552	2.1424	2.0958	2.2019	2.2841
100	2.6871	2.753	2.7278	2.6915	2.8147	2.8778
500	4.7351	4.7885	4.7222	4.7400	4.8890	4.9209
1000	6.0162	6.056	5.9651	6.0218	6.1773	6.2000
10^4	13.181	13.126	12.904	13.192	13.3565	13.358
10^5	28.613	28.332	27.834	28.639	28.7954	28.7779
10^6	61.860	61.074	59.990	61.915	62.0461	62.000

At the expense of a larger deviation from the exact solution for Sc = 1–2 (8 % at Sc = 1 and 4 % already at Sc = 2) Eq. (6.6) ensures only deviations of less than 1–3 % at higher Prandtl or Schmidt numbers (Fig. 6.1; Table 6.2).

For $Sc \to 0$, Eqs. (6.4)–(6.6) reduce to the asymptotic relation K_1/Sc = 0.885 [32]. For $Sc \to \infty$, they ensure agreement with another asymptotic $K_1 = 0.62 Sc^{1/3}$ [11, 32].

One more relation for K_1 for $Pr = 0{-}\infty$ was designed as a combination of asymptotic solutions for the cases $Pr \to 0$ and $Pr \to \infty$ [2]. Rewritten, using Sc number, this results in

$$K_1 = \left[(0.88447Sc)^{-1.077} + (0.62048Sc^{1/3})^{-1.077}\right]^{-1/1.077}. \tag{6.7}$$

For Sc = 2, Eq. (6.7) merges with the self-similar solution. Deviation of Eq. (6.7) from the exact solution grows up to 3.2 % at Sc = 2.5, exhibits a maximum of 5.6 % at $Sc \approx 20$ and, for larger Schmidt numbers, diminishes to 2.7 % at Sc = 1000 and 0.6 % at $Sc = 10^5$.

Over the range of $Sc < 2$, deviation of Eq. (6.7) from the exact solution changes its sign, and increases in absolute values being 3.4 % at Sc = 1 and 8.2 % at Sc = 0.1 (Table 6.2).

To conclude, preference should be rendered to that of Eqs. (6.4)–(6.7) that ensures the lowest inaccuracy at the Schmidt numbers specific for the problem is to be solved.

Application to electrochemistry problems. Levich [11] derived an asymptotic solution for convective diffusion for very large Schmidt numbers $Sc \gg 1$

$$K_1 = 0.62 Sc^{1/3}. \tag{6.8}$$

It coincides with the asymptotic solution for heat transfer for $Pr \gg 1$ given in [32].

Table 6.2 elucidates that Eq. (6.8) correlates well with the exact solution at $Sc > 500$ (deviation for $Sc = 500$ is 3.9 % and reduces to zero for $Sc \to \infty$). Equation (6.8) overruns the exact solution by 7.1 % at $Sc = 100$ and by 56.7 % at $Sc = 1$. Levich's Eq. (6.8) was successfully validated in experimental studies [4, 5, 7, 8, 12, 14] at high Schmidt numbers.

Rotating disk electrodes are intensively employed in experimental electrochemical investigations [1, 11]. Convective diffusion, which displays itself as the diffusion of the electrical current on the electrode, is modeled by Eq. (1.28).

For this case, Eq. (6.3) for laminar flow in view of Eq. (6.8) is usually rewritten as [1, 11]

$$i_{\mathrm{L}} = 0.62 n F C_{\mathrm{F}} C_{\infty} D_m^{2/3} \nu^{-1/6} \omega^{1/2}, \tag{6.9}$$

where i_{L} is the limiting diffusion current of electrons to the surface of a rotating disk electrode; n is the number of electrons that are involved in the current; F is the disk area; C_{F} is the Faraday constant (96,485 C/mol); C_{∞} is the concentration at infinity, mol/m^3. Based on this, one can ascertain that the mass transfer coefficient can be written as $\alpha_m = i_{\mathrm{L}}/(nFC_{\mathrm{F}}C_0)$, while Eq. (6.9) translates into Eq. (6.8).

In practice, the following tasks are actual: (1) searching a functional dependence of i_{L} on ω; (2) finding the diffusion coefficient D_m, whereas the value of i_{L} is measured; and (3) measurements of Volt–Ampere characteristics using a rotating disk electrode.

Naphthalene sublimation technique for experimental determination of the mass and heat transfer coefficients. Convective heat transfer from a surface to air is analogous to convective mass transfer in naphthalene sublimation to air. Naphthalene sublimation has been often employed to measure the average mass transfer of an *entire* disk weighted before and after the measurement to determine the amount of naphthalene lost by the disk as a result of experiments [19–21, 25–27]. Currently, accurate instrumentation is available for local pointwise scanning of the naphthalene layer thickness and subsequent calculation of local mass transfer coefficients for laminar, transitional, and turbulent flow [15–18, 22, 24, 28]. In frames of the analogy between the surface heat and mass transfer, constants K_1 in Eq. (3.4) for the Nusselt number and Eq. (6.3) for the Sherwood number can be expressed as [23]

$$K_1 = C\, Pr^{m_p}, \tag{6.10}$$

$$K_1 = C\, Sc^{m_p}, \tag{6.11}$$

where the coefficient C is identical in both equations. The effects of the Prandtl and Schmidt numbers are described by respective multipliers in Eqs. (6.10) and (6.11).

Equations (6.10) and (6.11) are used for the Prandtl and Schmidt numbers moderately diverging from unity: $Pr = 0.7–0.74$ for air, whereas $Sc = 2.28–2.5$ for naphthalene sublimation in air. Therefore, the constant C is assigned to be equal to the coefficient K_1 at $Sc = 1$ and $Pr = 1$ at T_w = const. or C_w = const. (see Table 6.1), i.e., $C = 0.3963$.

Authors [15–19, 24, 28] used the naphthalene sublimation technique to measure rotating disk mass transfer and set the exponent m_p to be the same for all values of Pr and Sc, which yields a relation between the Nu and Sh numbers

$$Nu/Sh = (Pr/Sc)^{m_p}. \tag{6.12}$$

The scatter of the values of the exponent m_p in the literature amounted up to 45 %: $m_p = 1/3$ [17], $m_p = 0.4$ [15, 17, 18, 20], $m_p = 0.53$ [19], and $m_p = 0.58$ [24].

Erroneous values m_p entail fallacious results of post-processing of the experimental data from the naphthalene sublimation technique aimed at estimation of heat transfer in air. An analysis and recommendation of the proper value m_p were made by the author [23].

Exponent m_p can be detected from the self-similar solution of the problem (Tables 3.1 and 6.1). Table 6.3 lists exponents m_p for the Prandtl/Schmidt numbers moderately deviating from unity [23]. It is evident from here that the function $m_p(Pr)$ exhibits a decreasing trend and varies from $m_p = 0.5723$ to $m_p = 0.5024$, if the Prandtl/Schmidt numbers grow from 0.7 up to 2.5. Consequently, the effective exponent $m_p = 0.53$ suggested in [19] is practically the average m_p value weighted over the range $Pr = 0.7–2.5$.

Figure 6.1 depicts different experimental data for the constant K_1 in naphthalene sublimation in air. These data agree well with the self-similar solution (see Table 6.2); only the too large value $K_1 = 0.69$ for $Sc = 2.5$ [24] falls out from the overall picture.

Table 6.3 Value m_p in Eqs. (6.10), (6.11) and (6.12) based on the exact solution of Eqs. (2.32)–(2.36) for laminar flow [23, 30]

Pr (Sc)	0.5	0.6	0.7	0.71	0.72	0.8	0.9	0.95	0.99
m_p	0.5954	0.5827	0.5723	0.5714	0.5705	0.5638	0.5571	0.5551	0.5632
Pr (Sc)	1.05	1.1	1.5	2	2.28	2.4	2.5	3	4
m_p	0.5438	0.5424	0.5264	0.5123	0.5064	0.5041	0.5024	0.4949	0.4841
Pr (Sc)	5	10	20	50					
m_p	0.4765	0.4566	0.4411	0.4251					

Post-processing [23] of the measured results using Eq. (6.12) at $m_p = 0.53$ to reduce them to conditions of heat transfer at $Pr = 0.71$ yields the values $K_1 = 0.325$ [17], $K_1 = 0.328$ [20, 21, 26], $K_1 = 0.331$ [19], $K_1 = 0.321$ [25], $K_1 = 0.322$ [22] that agree well with the exact value $K_1 = 0.326$ for $Pr = 0.71$ and T_w = const. (see Table 3.1) and reliable experimental data (see Chap. 3). Falling out of the overall good conformance are (a) the constant $K_1 = 0.318$ resulting from the low value $K_1 = 0.59$ in naphthalene sublimation at $Sc = 2.28$ measured in [15], and (b) the constant $K_1 = 0.354$ stemming from the high experimental value $K_1 = 0.69$ in naphthalene sublimation obtained in [24] (see Fig. 6.1).

The use of the value $m_p = 0.4$ suggested in [15, 17, 18, 20] and widely used throughout the literature brings for the heat transfer in air at $Pr = 0.71$ [23]: $K_1 = 0.37$ [15]; $K_1 = 0.379$ [17]; $K_1 = 0.384$ [20, 21, 26]; $K_1 = 0.388$ [19]; $K_1 = 0.378$ [25]; $K_1 = 0.380$ [22]; $K_1 = 0.417$ [24]. All these recalculated data are too large as compared to the exact value $K_1 = 0.326$.

Taking the exponent $m_p = 1/3$ [17], one can obtain for $Pr = 0.71$ [23] the constants $K_1 = 0.4$ [15]; $K_1 = 0.409$ [17]; $K_1 = 0.416$ [20, 21, 26]; $K_1 = 0.421$ [19]; $K_1 = 0.411$ [25]; $K_1 = 0.413$ [22]; $K_1 = 0.454$ [24]. They surpass the exact value $K_1 = 0.326$ to an even larger extent.

Involvement of the exponent $m_p = 0.58$ [24] yields for $Pr = 0.71$ the values $K_1 = 0.3$ [15], $K_1 = 0.307$ [17], $K_1 = 0.308$ [20, 21, 26], $K_1 = 0.311$ [19], $K_1 = 0.301$ [25], $K_1 = 0.303$ [22], that are too small [23]. Only the value $K_1 = 0.332$ [24] is acceptable, which is due to the high value $m_p = 0.58$ chosen by the authors [24] to agree with the exact solution $K_1 = 0.326$. However, it is clear that the too large exponent $m_p = 0.58$ results from the too large value $K_1 = 0.69$ in naphthalene sublimation measured in [24], which is discordant with the measurements of the other researchers.

Authors [25] rearranged Eq. (6.12) in the following way

$$Nu/Sh_{Sc=2.5} = f(Pr)Pr^{1/3}. \tag{6.13}$$

The value $K_1 = 0.625$ at $Sc = 2.5$ and function $f(Pr) = 0.576$, 0.634, 0.737, 0.842 and 0.926 at Pr = 0.1, 1, 2.5, 10 and 100, respectively, yield jointly the values $K_1 = 0.321$, 0.396, 0.625, 1.134 and 2.686 at the Prandtl numbers mentioned above. This is fully consistent with the self-similar solution at T_w = const. (Table 6.1, $n_* = 0$). The correction function $f(Pr)$ can be recast to incorporate the multiplier $Pr^{1/3}$. Use of Eq. (6.13) ensures higher accuracy than that conveyed by approaches operating with a single value of m_p, though Eq. (6.13) is less practical as Eq. (6.12), because of the involvement of a tabulated function.

To conclude, Eq. (6.12) with the exponent $m_p = 0.53$ [19] can be suggested as the most accurate and practical one for post-processing of the measured laminar mass transfer coefficients of a rotating disk in naphthalene sublimation in air in order to recalculate it to laminar heat transfer in air. As an alternative, Eq. (6.13) (or its modification) can be used.

6.2 Transitional and Turbulent Flow for the Prandtl and Schmidt Numbers Moderately Different from Unity

Values of $Pr \le 5$ and $Sc \le 5$ are considered here as those moderately deviating from unity. The objective is again a validation of the experimental technique dealing with sublimation of naphthalene from a rotating disk in air at Sc = 2.28–2.5 [23].

Local Sherwood numbers in naphthalene sublimation experiments in air in transitional and turbulent flow obtained in the recent works [15, 18] together with the data for laminar flow and different empirical approximations are depicted in Fig. 6.2. Recast Eq. (3.13) [15] for transitional flow (corrected range of validity) and empirical equations [15, 18] for turbulent flow look as follows [15, 18]

$$Sh = 2.0 \times 10^{-19} Re_\omega^4 \quad \text{for} \quad Re_\omega = (1.9{-}2.75) \times 10^5 \text{ (Ref. [15])}, \tag{6.14}$$

$$Sh = 0.0512 Re_\omega^{0.8} \quad \text{for} \quad Re_\omega \ge 2.75 \times 10^5 \text{ (Ref. [15])}, \tag{6.15}$$

$$Sh = 0.0518 Re_\omega^{0.8} \quad \text{for} \quad Re_\omega \ge 2.5 \times 10^5 \text{ (Ref. [18])}. \tag{6.16}$$

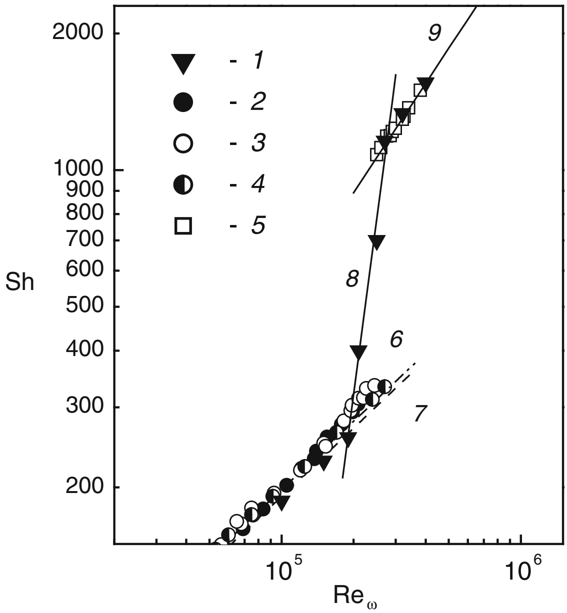

Fig. 6.2 Local Sherwood numbers for naphthalene sublimation in air [23, 30]. Experiments: *1*—Sc = 2.28 [15]; *2*—Sc = 2.4 [21]; *3*—Sc = 2.4 [26]; *4*—Sc = 2.44 [19]; *5*—Sc not mentioned [18]. Empirical approximations, Eq. (6.3): *6*—laminar flow, $n_R = 1/2$, $K_1 = 0.625$ [20, 21, 25, 26]; *7*—laminar flow, $n_R = 1/2$, $K_1 = 0.604$ [17]; *8*—transitional flow, $n_R = 4$, $K_1 = 2 \times 10^{-19}$, Eq. (6.14) [15]; *9*—turbulent flow, $n_R = 0.8$, $K_1 = 0.0512$, Eq. (6.15) [15]

In practice, one often needs to estimate average Sherwood numbers Sh_{av} (or average Nusselt numbers Nu_{av}) of an *entire* disk, where areas occupied by laminar/transitional flow or laminar/transitional/turbulent flow emerge at the same time. For instance, only surface-averaged mass transfer coefficients of an *entire* disk were measured in [19–21, 25, 26].

Measurements of the average Sherwood number over an *entire* disk covered with areas of laminar, transitional and turbulent flow were performed by [19–21, 25, 26]. Reynolds analogy between mass transfer and fluid flow was involved to derive a quite inconvenient theoretical solution for Sh_{av} for an entire disk [21, 26] incorporating parameters, which were rather difficult to determine by means of the used approach. More promising is the model for Sh_{av} first used in the paper [7] and further generalized by the author of the present work [23, 30], which enables verifications of the recent measurements of the local Sherwood numbers by means of comparisons with the vast database for the average Sherwood numbers for an *entire* disk.

The author [7] assumed that laminar-turbulent transition sets on instantly at a radial coordinate r_{tr} corresponding to the Reynolds number $Re_{\omega,tr}$. Subsequently, the value Sh_{av} for an entire disk can be found using the following integral

$$Sh_{av} = \frac{2}{b}\left[\int_0^{r_{tr}} Sh_{lam}\mathrm{d}r + \int_{r_{tr}}^{b} Sh_{turb}\mathrm{d}r\right]. \tag{6.17}$$

Sherwood numbers are presented by Eq. (6.3) accompanied with the constants $K_{1,lam}$ and $n_R = 1/2$ for laminar flow, and $K_{1,turb}$ and $n_R = 0.8$ for turbulent flow. An integration of Eq. (6.17) yields

$$Sh_{av} = K_{1,lam}Re_{\omega,tr}^{1/2}\left(\frac{Re_{\omega,tr}}{Re_{\varphi}}\right)^{1/2} + \frac{2}{2n_R+1}K_{1,turb}Re_{\varphi}^{n_R}\left[1-\left(\frac{Re_{\omega,tr}}{Re_{\varphi}}\right)^{n_R+1/2}\right]. \tag{6.18}$$

If $Re_{\varphi} < Re_{\omega,tr}$, the second summand in Eq. (6.18) must be discarded. Asymptotically at $Re_{\varphi} \gg Re_{\omega,tr}$, Eq. (6.18) degenerates to Eq. (6.3) for turbulent flow with

$$K_{2,turb} = \frac{2}{2n_R+1}K_{1,turb}. \tag{6.19}$$

Given $n_* = 0$, which effectively means T_w = const. and C_w = const., Equation (6.18) translates into Eq. (3.25), while Eq. (6.19) turns to Eq. (3.35) in view of the relation $2n_R = 1 + m$ resulting from Eqs. (2.78) and (3.31).

In [12] it is suggested taking into account regions of laminar, transitional and turbulent flow separately. If the transition sets on at the radial location r_{tr1} (or at

$Re_{\omega,\mathrm{tr1}}$) and ends at the radial location r_{tr2} (or $Re_{\omega,\mathrm{tr2}}$), a definite integral for Sh_{av} can be written as

$$Sh_{\mathrm{av}} = \frac{2}{b}\left[\int\limits_{0}^{r_{\mathrm{tr1}}} Sh_{\mathrm{lam}}\mathrm{d}r + \int\limits_{r_{\mathrm{tr1}}}^{r_{\mathrm{tr2}}} Sh_{\mathrm{tran}}\mathrm{d}r + \int\limits_{r_{\mathrm{tr2}}}^{b} Sh_{\mathrm{turb}}\mathrm{d}r\right]. \tag{6.20}$$

The transitional Sherwood number Sh_{tran} is specified by the first of Eq. (6.3) complemented with experimental values of $K_{1,\mathrm{tran}}$ and $n_{\mathrm{R,tran}}$ for transitional flow. Integration of Eq. (6.20) results in

$$\begin{aligned} Sh_{\mathrm{av}} = {} & K_{1,\mathrm{lam}} Re_{\omega,\mathrm{tr1}}^{1/2}\left(\frac{Re_{\omega,\mathrm{tr1}}}{Re_{\varphi}}\right)^{1/2} + \frac{2}{2n_{\mathrm{R,tran}}+1} K_{1,\mathrm{tran}} Re_{\omega,\mathrm{tr2}}^{n_{\mathrm{R,tran}}}\left(\frac{Re_{\omega,\mathrm{tr2}}}{Re_{\varphi}}\right)^{1/2} \\ & \times\left[1-\left(\frac{Re_{\omega,\mathrm{tr1}}}{Re_{\omega,\mathrm{tr2}}}\right)^{n_{\mathrm{R,tran}}+1/2}\right] + \frac{2}{2n_{\mathrm{R}}+1} K_{1,\mathrm{turb}} Re_{\varphi}^{n_{\mathrm{R}}}\left[1-\left(\frac{Re_{\omega,\mathrm{tr2}}}{Re_{\varphi}}\right)^{n_{\mathrm{R}}+1/2}\right]. \end{aligned} \tag{6.21}$$

Equation (6.21) holds at $Re_{\varphi} \geq Re_{\omega,\mathrm{tr2}}$. If $Re_{\varphi} < Re_{\omega,\mathrm{tr2}}$, the last term in Eq. (6.21) is discarded, whereas the second summand turns to

$$\begin{aligned} Sh_{\mathrm{av}} = {} & K_{1,\mathrm{lam}} Re_{\omega,\mathrm{tr1}}^{1/2}\left(\frac{Re_{\omega,\mathrm{tr1}}}{Re_{\varphi}}\right)^{1/2} \\ & + \frac{2}{2n_{\mathrm{R,tran}}+1} K_{1,\mathrm{tran}} Re_{\varphi}^{n_{\mathrm{R,tran}}}\left[1-\left(\frac{Re_{\omega,\mathrm{tr1}}}{Re_{\varphi}}\right)^{n_{\mathrm{R,tran}}+1/2}\right]. \end{aligned} \tag{6.22}$$

Asymptotically for $Re_{\varphi} \gg Re_{\omega,\mathrm{tr2}}$, Eq. (6.21) transforms to the second of Eq. (6.3), whereas the constant $K_{2,\mathrm{turb}}$ is given by Eq. (6.19). A solution derived in [12] is a particular case of Eq. (6.21), whose empirical constants resulting from experiments [12] at high Sc numbers are fixed numerical values. Hence, the solution [12] as it is can not be used to describe the experimental data for naphthalene sublimation.

Substitution of numerical values of the constants resulting from measurements at naphthalene sublimation in air [15] (see Eqs. (6.14), (6.15) and caption to Fig. 6.1) into the general Eqs. (6.18)–(6.22) yields

(a) applied to Eq. (6.18)

$$Sh_{\mathrm{av}} = 0.59 Re_{\omega,\mathrm{tr}}^{1/2}\left(\frac{Re_{\omega,\mathrm{tr}}}{Re_{\varphi}}\right)^{1/2} + \frac{2}{2.6} 0.512 Re_{\varphi}^{0.8}\left[1-\left(\frac{Re_{\omega,\mathrm{tr}}}{Re_{\varphi}}\right)^{1.3}\right], \tag{6.23}$$

(b) applied to Eq. (6.19)

$$K_{2,\mathrm{turb}} = \frac{2}{2.6} K_{1,\mathrm{turb}} = 0.0394, \tag{6.24}$$

(c) applied to Eq. (6.21)

$$\begin{aligned} Sh_{\mathrm{av}} &= 0.59 \times 1.9 \times 10^5 \times Re_{\varphi}^{-1/2} + \frac{4}{9} 10^{-19} (2.75 \times 10^5)^{4.5} \\ &\quad \times Re_{\varphi}^{-1/2} \left[1 - \left(\frac{1.9 \times 10^5}{2.75 \times 10^5} \right)^{4.5} \right] \\ &\quad + 0.0394 Re_{\varphi}^{0.8} \left[1 - \left(\frac{2.75 \times 10^5}{Re_{\varphi}} \right)^{1.3} \right], \quad Re_{\varphi} \geq 2.75 \times 10^5, \end{aligned} \tag{6.25}$$

(d) applied to Eq. (6.22)

$$\begin{aligned} Sh_{\mathrm{av}} &= 0.59 \times 1.9 \times 10^5 \times Re_{\varphi}^{-1/2} + \frac{4}{9} 10^{-19} Re_{\varphi}^{4} \left[1 - \left(\frac{1.9 \times 10^5}{Re_{\varphi}} \right)^{4.5} \right], \\ Re_{\varphi} &= (1.9\text{–}2.75) \times 10^5. \end{aligned} \tag{6.26}$$

The Reynolds number $Re_{\omega,\mathrm{tr}}$ (instant transition to turbulence) in Eq. (6.23) remains a free parameter to be tuned for a better agreement with particular experiments.

Figure 6.3 shows validations of Eqs. (6.23)–(6.28) by comparison with experimental data. Experimental data 1, 5 and curve 6 for Sh_{av} for purely turbulent flow stem from the works [23, 30] and result from reprocessing of the measured data [15, 18] and Eq. (6.15) using Eq. (6.24). For laminar flow, we have $K_{2,\mathrm{lam}} = K_{1,\mathrm{lam}}$ (curves 7 and 8). Curve 9 combining Eqs. (6.25), (6.26) and incorporating boundaries of transitional flow conforms to experiments [19, 21, 26] for Sh_{av} for an *entire* disk depicted in Fig. 6.3.

In Fig. 6.3, experimental data 1 for Sh_{av} for an *entire* disk were calculated in [23] using Eqs. (6.25), (6.26) and measurements [15] for laminar, transitional and turbulent flow. These data points go beyond curve 9 at respective values of the argument Re_{φ}.

The replacement of the Reynolds number $Re_{\omega,\mathrm{tr}}$ in Eq. (6.23) (instant transition to turbulence) with its values at the onset and end of transition (i.e., 1.9×10^5 and 2.75×10^5) yields curves 10 and 11 lying above and below curve 9, respectively. Reynolds number of the instant transition to turbulence $Re_{\omega,\mathrm{tr}} = 2.35 \times 10^5$, an arithmetic mean of values $Re_{\omega,\mathrm{tr1}}$ and $Re_{\omega,\mathrm{tr2}}$, substituted into Eq. (6.23) conveyed curve 12, which agrees with curve 9.

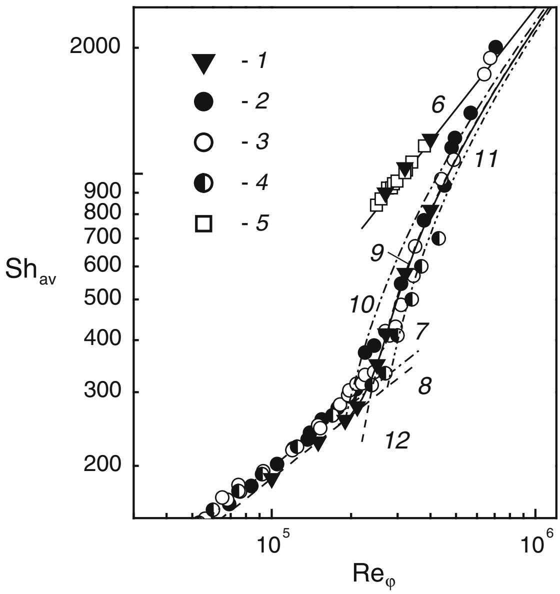

Fig. 6.3 Average Sherwood numbers, naphthalene sublimation in air [23, 30]. Experiments: *1*—Sc = 2.28 [15]; *2*—Sc = 2.4 [21]; *3*—Sc = 2.4 [26]; *4*—Sc = 2.44 [19]; *5*—Sc not mentioned [18]. Calculation, Eq. (6.3): *6*—turbulent flow, $n_R = 0.8$, $K_2 = 0.0394$, Eq. (6.24) [15]; *7*—laminar flow, $n_R = 1/2$, $K_1 = 0.625$ [20, 21, 25, 26]; *8*—laminar flow, $n_R = 1/2$, $K_1 = 0.59$ [15]. Calculation of Sh_{av} for the *entire* disk: *9*—Eqs. (6.25) and (6.26); *10*—Eq. (6.23) at $Re_{\omega,tr} = 1.9 \times 10^5$; *11*—Eq. (6.23) at $Re_{\omega,tr} = 2.75 \times 10^5$; *12*—Eq. (6.23) at $Re_{\omega,tr} = 2.35 \times 10^5$

In the asymptotic case of $Re_\varphi \to \infty$, lines 9–12 coincide with curve 6 valid for purely turbulent flow.

Thus, Eqs. (6.21) and (6.22) incorporating terms accounting for the coexistence of laminar, transitional and turbulent flow areas ensure the best agreement with experiments for the Sh_{av} number for an *entire* disk. Equation (6.18) resulting from a simpler model [7] ensures the efficiency similar to that of Eqs. (6.21) and (6.22), if an "effective" Reynolds number $Re_{\omega,tr}$ of the instant transition to turbulent flow is chosen correctly.

Application to the naphthalene sublimation technique. Again, a recalculation of the mass transfer to heat transfer data is performed using Eq. (3.4) and (6.3), with the constants K_1 defined in Eqs. (6.10) and (6.11), accordingly [23]. The factor C is equal to the constant K_1 for $Sc = 1$, $Pr = 1$ under conditions T_w = const. or C_w = const.

Authors [15, 18] used the constant $m_p = 0.4$ for a turbulent flow regime and $Pr = Sc = 0.7$–2.5. Equation (6.12) at $m_p = 0.4$ yields the value $K_1 = 0.0323$ for heat transfer in air at T_w = const. and $Pr = 0.72$, starting from the values $K_1 = 0.0512$–0.0518 (see Eqs. (6.15) and (6.16)) for $Sc = 2.28$ as a base for the recalculation. But, in reality, experiments [35–37] (see Table 3.5) conveyed the value of the constant $K_1 = 0.0188$ at T_w = const. and $Pr = 0.72$. The theoretical model [38, 39] gave the value K_1 = 0.0187 for the same conditions. Thus, also for turbulent flow, an erroneous value m_p leads to fallacious translation of the naphthalene sublimation data to heat transfer in air.

Equations (6.10), (6.11) are to be used for the Prandtl and Schmidt numbers moderately diverging from unity: Pr = 0.7–0.74 for air; Sc = 2.28–2.5 for naphthalene sublimation. Hence, the constant C in Eqs. (6.10), (6.11) must be equal to the coefficient $K_1 = 0.0232$ in turbulent flow at Sc = 1, Pr = 1 and conditions T_w = const., C_w = const. (Table 3.7).

Detecting of the exponent m_p for turbulent flow is performed using experimental data. Only experimental Eqs. (6.15) and (6.16) [15, 18] can serve for this purpose. Based on Eq. (6.15) as well as the values C = 0.0232, K_1 = 0.0188 (at T_w = const. and Pr = 0.72) [35–37], one can transform Eqs. (6.10) and (6.11) as follows

$$K_1 = 0.0232 Pr^{0.64} \quad \text{for } Pr \le 1, \tag{6.27}$$

$$K_1 = 0.0232 Sc^{0.96} \quad \text{for } Sc \ge 1. \tag{6.28}$$

This means that the exponent m_p for turbulent flow is not universal being a function of the Prandtl and Schmidt numbers, which apparently results from different effects of the Pr or Sc larger and smaller than unity. Equations (6.27) and (6.28) yield as a result

$$Nu/Sh = Pr^{0.64}/Sc^{0.96}. \tag{6.29}$$

Using the idea of a correction function, Eq. (6.13), one can transform Eq. (6.29) as

$$Nu/Sh_{Sc=2.28} = f(Pr). \tag{6.30}$$

At Pr = 0.72, the correction function $f(Pr)$ takes the value $f(Pr)$ = 0.367.

As an alternative, one can use an effective value of the exponent m_p so that

$$Nu/Sh = (Pr/Sc)^{0.87}. \tag{6.31}$$

The exponent m_p = 0.87 in Eq. (6.31) is more than twice larger than the value 0.4 mistakenly recommended in [15, 18]. Nevertheless, the value m_p = 0.87 must not be used in Eqs. (6.27) and (6.28) to avoid significant errors in predictions of the constant K_1.

The empirical Eq. (3.10) [37] for transitional flow at T_w = const. and Pr = 0.72 is the most appropriate to be used jointly with Eq. (6.14) for transitional flow at C_w = const. Thus, Eq. (6.12) should be recast in view of Eqs. (3.10) and (6.14) as follows

$$Nu/Sh = (Pr/Sc)^{0.6}. \tag{6.32}$$

Equation (3.10) is valid for $Re_\omega = 1.95 \times 10^5$–$2.5 \times 10^5$, while Eq. (6.14) holds at $Re_\omega = 1.9 \times 10^5$–$2.75 \times 10^5$. These differences are though rather insignificant.

To conclude, Eqs. (6.29)–(6.31) should be employed to recalculate the data for turbulent mass transfer for naphthalene sublimation in air to the conditions of heat transfer in air. Equation (6.32) should be applied for transitional flow for the same purpose [23].

6.3 Transitional and Turbulent Flow at High Schmidt Numbers

High values of the Schmidt numbers can be encountered in electrochemistry problems: Sc = 34–10,320 [4, 5, 7, 8, 12]. Main objectives of this section are validation and development of recommendations for the further use of the experimental and theoretical data of different authors [40].

Experimental data [7] for average Sherwood numbers for an entire disk at $Re_\varphi = 0.278 \times 10^6$–$1.8 \times 10^6$, Sc = 930–10,320 were described by a relation

$$Sh_{av} = Sc^{1/3} Re_\varphi^{-1/2} [0.62 Re_{\omega,tr} + 1.08 \times 10^{-2} (Re_\varphi^{1.37} - Re_{\omega,tr}^{10.37})]. \tag{6.33}$$

Here, Eq. (6.18) at $K_{1,lam} = 0.62 Sc^{1/3}$, $K_{1,turb} = 0.0148 Sc^{1/3}$, $Re_{\omega,tr} = 2.78 \times 10^5$ and $n_R = 0.87$ was taken into account. In the transitional region at $Re_\omega = 2.3 \times 10^5$–$2.9 \times 10^5$, Eq. (6.33) lies below the experimental data [7] (in analogy to curve 12 in Fig. 6.3), which results from simplifications incorporated in model (6.18) and mentioned in Sect. 6.2.

A reduced form of Eq. (6.33) for purely turbulent flow [7] and an equation for the local Sherwood numbers derived in [30, 40] have the following form

$$Sh_{av} = 1.08 \times 10^{-2} Re_\varphi^{0.87} Sc^{1/3}, \tag{6.34}$$

$$Sh = 1.48 \times 10^{-2} Re_\omega^{0.87} Sc^{1/3}. \tag{6.35}$$

Measurements [4] of the average Sherwood numbers for an entire disk performed at $Re_\varphi = 5 \times 10^4$–$1.8 \times 10^6$, Sc = 345–6450 (transition at $Re_\varphi = 2.3 \times 10^5$–$2.9 \times 10^5$) for the region of turbulent flow were described by the relation

$$Sh_{av} = 0.0725 Re_\varphi^{0.9} Sc^{0.33}. \tag{6.36}$$

The authors [5] measured local Sh and average Sh_{av} numbers at laminar, transitional, and turbulent flow for $Re_\omega = 4 \times 10^4$–$2.2 \times 10^6$, Sc = 680–7200 (transition at $Re_\omega = 2.2 \times 10^5$–$3.0 \times 10^5$). Sherwood numbers for the turbulent flow [5] and average values for an entire disk (approximated in [30]) are given by the following relations, respectively

$$Sh = 1.09 \times 10^{-2} Re_{\omega}^{0.91} Sc^{1/3}, \tag{6.37}$$

$$Sh_{\mathrm{av}} = 7.67 \times 10^{-3} Re_{\varphi}^{0.91} Sc^{1/3}, \tag{6.38}$$

$$Sh_{\mathrm{av}} = Sc^{1/3} Re_{\varphi}^{-1/2} [0.62 Re_{\omega,\mathrm{tr}} + 7.67 \times 10^{-3} (Re_{\varphi}^{1.41} - Re_{\omega,\mathrm{tr}}^{1.41})], \tag{6.39}$$

where the Reynolds number of the abrupt transition was $Re_{\omega,\mathrm{tr}} = 2.78 \times 10^5$ [7].

Experiments [8] for Sh_{av} for an entire disk were performed at $Re_{\varphi} = 10^4$–1.18×10^7, $Sc = 34$–1400. For purely turbulent flow at $Re_{\varphi} = 8.9 \times 10^5$–$1.18 \times 10^7$, authors [8] obtained

$$Sh_{\mathrm{av}} = 1.17 \times 10^{-2} Re_{\varphi}^{0.896} Sc^{0.249}. \tag{6.40}$$

Experiments for the local Sherwood numbers in transitional flow at $Re_{\omega} = 2.0 \times 10^5$–$3.0 \times 10^5$ and $Sc = 1192$–2465 were described by the empirical Eq. (3.14) [12].

The authors [12] deduced empirical equations for Sh_{av} for turbulent flow (based on experiments [4]), simultaneous existence of laminar and transitional flow, as well as simultaneous existence of laminar, transitional and turbulent flow, respectively

$$Sh_{\mathrm{av}} = 7.8 \times 10^{-3} Re_{\varphi}^{0.9} Sc^{1/3}, \tag{6.41}$$

$$Sh_{\mathrm{av}} = Sc^{1/3} Re_{\varphi}^{-1/2} [0.89 \times 10^5 + 9.7 \times 10^{-15} Re_{\varphi}^{3.5}], \tag{6.42}$$

$$Sh_{\mathrm{av}} = Sc^{1/3} Re_{\varphi}^{-1/2} [7.8 \times 10^{-3} Re_{\varphi}^{1.4} - 1.3 \times 10^5]. \tag{6.43}$$

Equations (6.42) and (6.43) are particular cases of Eqs. (6.22) and (6.21), accordingly, with Eq. (6.8) used for laminar, Eq. (3.14) for transitional and Eq. (6.41) for turbulent flow.

Theoretical solutions for the local turbulent Sherwood numbers at high Schmidt numbers derived in [9, 41] can be presented as follows, respectively,

$$Sh_{\mathrm{av}} = 7.07 \times 10^{-3} Re_{\varphi}^{0.9} Sc^{1/3}, \tag{6.44}$$

$$Sh_{\mathrm{av}} = 5.93 \times 10^{-3} Re_{\varphi}^{0.91} Sc^{0.34}. \tag{6.45}$$

A theoretical solution obtained in [10] coincides with Eq. (6.41). The solution obtained in [42] has a form of Eq. (6.41) with the coefficient changed to 6.43×10^{-3}.

In [43] a theoretical solution claimed to be valid for $Sc = 0.72$–∞ has been proposed, however, as demonstrated in [30, 40], this relation is inaccurate.

Some of the theoretical and empirical relations for the Sherwood numbers for purely turbulent flow, as well as for average Sh_{av} numbers for an entire disk

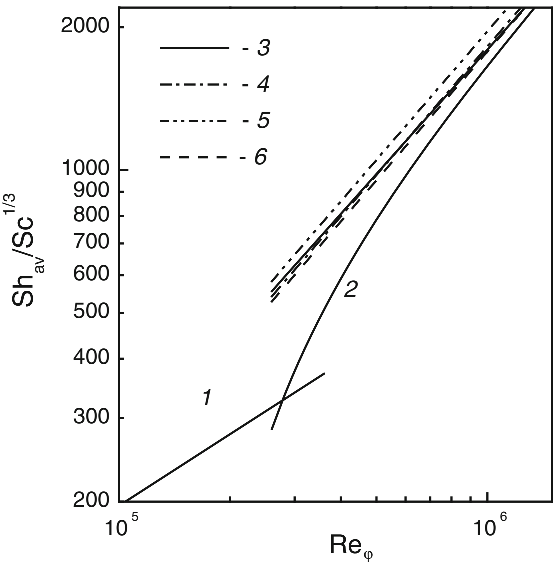

Fig. 6.4 Average Sherwood numbers at high Schmidt numbers [30]. Approximation of experiments: *1*—laminar flow, Levich's Eq. (6.8); *2*—Eq. (6.33) for an *entire* disk [7]; *3*—Eq. (6.34) [7]; *4*—Eq. (6.36) [4]; *5*—Eq. (6.41) [10, 12]. Theoretical solution: *6*—Eq. (6.44) [9]

simultaneously occupied by laminar, transitional, and turbulent flow areas agree well with each other. Curves by Eqs. (6.34), (6.36), (6.44), and (6.45) practically merge (see Fig. 6.4). Equation (6.41) significantly surpasses original experiments [4]; corrected coefficient 6.43 × 10^{-3} [42] shifts predictions by Eq. (6.41) 9 % below those by Eq. (6.44). Empirical Eqs. (6.34) and (6.36) practically coincide, which corroborates the reliability of these experiments.

Equation (6.38) for turbulent flow and Eq. (6.39) for an entire disk significantly surpass Eqs. (6.33) and (6.34), respectively (see Fig. 6.5). Only in Eq. (6.40) [8], exponent 0.249 at the Schmidt number is not equal to 1/3. The large scatter of experiments around the approximation curve [8] is rather an evidence that the exponent 0.249 is erroneous. As demonstrated in [30, 40], differences between the curves by Eq. (6.40) plotted in the relation $Sh_{\text{av}}/Sc^{1/3}$ versus Re_φ for different Sc values revealed in experiments [8] is rather significant. Hence, Eq. (6.40) should be discarded as too inaccurate.

The exponent for the Reynolds number Re_φ in Eq. (6.35) diverges from those in Eqs. (6.15) and (6.16). Equation (6.35) can be recast to make the exponent for Re_φ equal to 0.8. This yields for the entire disk [30, 40]

$$Sh_{\text{av}}Sc^{-1/3} = 0.62Re_{\omega,tr}^{1/2}\left(\frac{Re_{\omega,tr}}{Re_\varphi}\right)^{1/2} + \frac{2}{20.6}0.0365Re_\varphi^{0.8}\left[1 - \left(\frac{Re_{\omega,tr}}{Re_\varphi}\right)^{1.3}\right]. \tag{6.46}$$

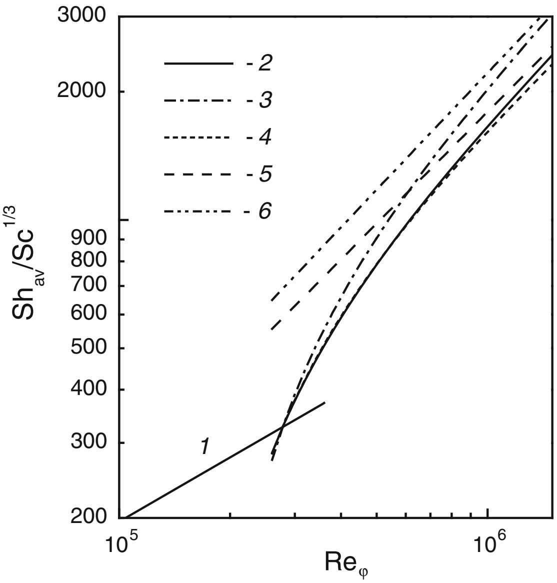

Fig. 6.5 Average Sherwood numbers at high Schmidt numbers, approximation of experiments [30]. *1*—laminar flow, Levich's Eq. (6.8); *2*—Eq. (6.33) for an *entire* disk [7]; *3*—Eq. (6.39), *entire* disk; *4*—Eq. (6.46), *entire* disk; *5*—Eq. (6.34) [7]; *6*—Eq. (6.38) [5]

Figure 6.5 depicts curves 2 and 4 plotted by Eqs. (6.33) and (6.46), respectively. Here again $Re_{\omega,\mathrm{tr}} = 2.78 \times 10^5$, like in Eq. (6.33). Curves 2 and 4 in fact merge for $Re_\varphi \le 9.0 \times 10^5$; deviations start to become visible for $Re_\varphi > 9.0 \times 10^5$.

For purely turbulent flow, Eq. (6.46) reduces asymptotically to the relations

$$Sh = 3.65 \times 10^{-2} Re_\omega^{0.8} Sc^{1/3}, \tag{6.47}$$

$$Sh_{\mathrm{av}} = 3.65 \times 10^{-2} \frac{2}{2.6} Re_\varphi^{0.8} Sc^{1/3} = 2.81 \times 10^{-2} Re_\varphi^{0.8} Sc^{1/3}. \tag{6.48}$$

Figure 6.6 demonstrates that Eq. (6.35) [7] used at $Sc = 2.28$ predicts Sherwood numbers close to the experiments [15, 18] for naphthalene sublimation in air and their approximation Eq. (6.15). Equations (6.35) (curve 10) and (6.15) (curve 9) correlate well at larger Reynolds numbers $Re_\omega = 0.6 \times 10^6$–$2.0 \times 10^6$. Curve 11, Eq. (6.47), lies in the vicinity of curve 10 at smaller Reynolds numbers $Re_\omega \le 0.7 \times 10^6$. Equation (6.47) yields $K_1 = 0.048$ at $Sc = 2.28$, which is only 6.7 % below the value $K_1 = 0.0512$ in Eq. (6.15). Curve 12 by Eq. (6.37) goes noticeably beyond experiments and approximation curve 9 in Fig. 6.6.

Dependence 13 in Fig. 6.6 plotted by experimental Eq. (3.14) [12] for transitional flow at $Sc = 2.28$ conforms well to Eq. (6.14) and experiments [15].

To conclude, the most reliable empirical relations for developed turbulent flow and an *entire* disk relying on the analysis made above are Eqs. (6.33)–(6.36).

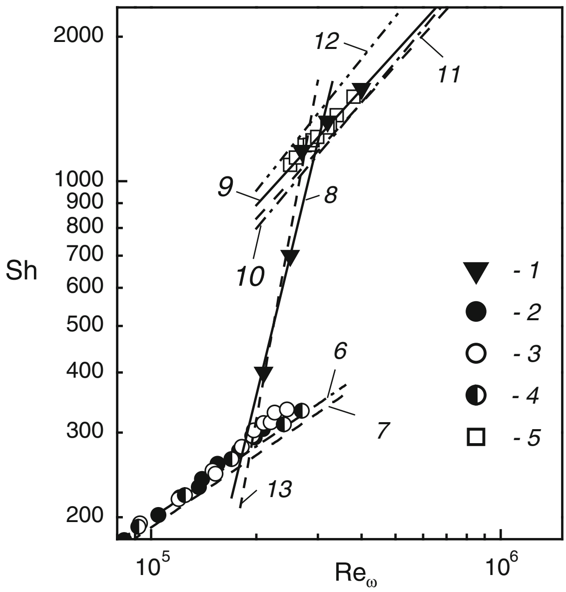

Fig. 6.6 Local Sherwood numbers for naphthalene sublimation [30]. Experiments: *1*—*Sc* = 2.28 [15]; *2*—*Sc* = 2.4 [21]; *3*—*Sc* = 2.4 [26]; *4*—*Sc* = 2.44 [19]; *5*—*Sc* not mentioned [18]. Empirical Eq. (6.3): *6*—laminar flow, n_R = 1/2, K_1 = 0.625 [20, 25, 26]; *7*—laminar flow, n_R = 1/2, K_1 = 0.604 [17]; *8*—transitional flow, n_R = 4, $K_1 = 2 \times 10^{-19}$ [15]; *9*—turbulent flow, n_R = 0.8, K_1 = 0.0512 [15]. Developed turbulent flow, *Sc* = 2.28: *10*—Eq. (6.35) [7]; *11*—Eq. (6.47); *12*—Eq. (6.37) [5]. Transitional flow, *Sc* = 2.28: *13*—Eq. (3.14) [12]

6.4 An Integral Method for *Pr* and *Sc* Numbers Much Larger Than Unity

Model with a constant value $\Delta \ll 1$. The thickness of the thermal (or diffusion) boundary layer at very high *Pr* or *Sc* numbers is much smaller than the thickness of the velocity boundary layer (i.e., $\Delta \ll 1$.). Hence, in Eq. (3.40) obtained for Δ = const. and $T^+ \equiv T^+(y^+)$, all summands in the parentheses in its left-hand part but a_* tend to zero

$$\Delta^{2n+1} a_* = \frac{4+m}{4+m+n_*}(a_* - 2b_* + c_*)Pr^{-n_p}. \tag{6.49}$$

Relying on Eq. (6.49), one can derive analytical solutions for constants Δ and K_1

$$\Delta = \left[\frac{4+m}{4+m+n_*}\left(1 - \frac{2D_3}{C_2}\right)\right]^{\frac{1}{2n+1}} Pr^{-\frac{n_p}{2n+1}}, \tag{6.50}$$

$$K_1 = K_3\left[\frac{4+m}{4+m+n_*}\left(1-\frac{2D_3}{C_2}\right)\right]^{\frac{-n}{2n+1}} Pr^{1+n_{\rm p}\left(\frac{n}{2n+1}-1\right)}, \tag{6.51}$$

where the coefficients C_2 and D_3 are described in the comments to Eqs. (2.68) and (2.69).

The cumulative exponent at the Prandtl number in Eq. (6.51) for $Pr \gg 1$ must be equal to 1/3 (see Sect. 6.3), which yields the following expression for $n_{\rm p}$

$$n_{\rm p} = \frac{2}{3}\cdot\frac{2n+1}{n+1}. \tag{6.52}$$

As a result, the constants K_1 and K_2 in view of Eq. (3.35) can be written as

$$K_1 = K_3\left[\frac{4+m}{4+m+n_*}\left(1-\frac{2D_3}{C_2}\right)\right]^{\frac{-n}{2n+1}} Pr^{1/3}, \tag{6.53}$$

$$K_2 = K_3\left[\frac{4+m}{4+m+n_*}\left(1-\frac{2D_3}{C_2}\right)\right]^{\frac{-n}{2n+1}} \frac{n_*+2}{2+n_*+m} Pr^{1/3}. \tag{6.54}$$

To enable validations against electrochemical experiments, let us further treat the Sherwood numbers rather than the Nusselt numbers and replace *Pr* with *Sc*.

In Fig. 6.7, Eq. (6.54) for $Sh_{\rm av}$ (at $n_* = 0$) is validated against the empirical Eq. (6.34) [7] and theoretical Eq. (6.44) [9]. Curves 5 and 6 predicted by Eq. (6.54) at $n = 1/7$ and 1/9 lie 20–30 % below the curves 3 and 4 suggested by Eqs. (6.34) and (6.44), accordingly. Such a discrepancy between theory and measurements is

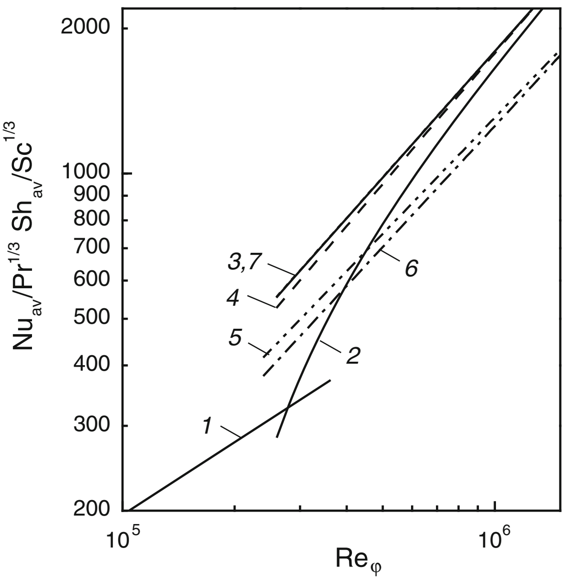

Fig. 6.7 Average Sherwood numbers for high Schmidt numbers [30]. Approximation of experiments: *1*—laminar flow, Levich's Eq. (6.8) [11]; *2*—Eq. (6.33) for an *entire* disk [7]; *3*—Eq. (6.34) [7] Theoretical solutions: *4*—Eq. (6.44) [9]; *5*—Eq. (6.54) for $n = 1/7$; *6*—Eq. (6.54) for $n = 1/9$; *7*—Eq. (6.73)

too high. In addition, the slope of the curves 5 and 6 (exponents at Re_φ being 0.8 and 0.833, constants K_2 being 0.0207 and 0.0126, accordingly) distinctly deviates from the slope of curves 3 and 4 (exponents at Re_φ being 0.87 and 0.9, constants K_2 being 0.0207 and 0.126, accordingly). Therefore, some model approaches incorporated in the present integral method partially fail at high *Pr* and *Sc* numbers and need to be improved. In Eq. (3.32) for the coefficient K_1, the total exponent at the Reynolds number can be increased, provided that the relative thickness Δ is assigned to be a decreasing function of the local Reynolds number Re_ω.

***Model with a variable value of* Δ.** The present integral method incorporates a model, in frames of which a boundary layer consists two parts. In the vicinity of the wall, a viscous and heat conduction sub-layers emerge, where the velocity and temperature profiles are described by Eq. (2.62). In the main part of the boundary layer (outside of the viscous sub-layer), velocity components are described by the power-law functions (see Chaps. 2 and 3). If Prandtl and Schmidt numbers are slightly different from unity, the thermal/diffusion and velocity boundary layers have a thickness of the same order of magnitude [30, 40]. Hence, integration of Eq. (2.23) for the thermal boundary layer has been performed over the *entire* velocity boundary layer. Viscous and heat conduction sub-layers are not taken into account in this integration, because they are negligibly thin in comparison with the overall boundary layer thickness. Velocity profiles in Eqs. (2.17)–(2.19) are integrated in the same way [31, 38, 39, 44, 45].

At very high Prandtl and Schmidt numbers, the boundary layer structure changes drastically. A very thin thermal/diffusion boundary layer is fully incorporated inside

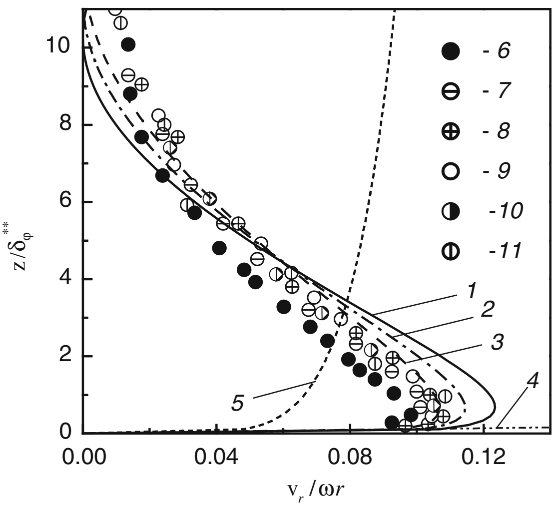

Fig. 6.8 Radial velocity profiles in the turbulent boundary layer over a free rotating disk [30]. *1*—n = 1/7; *2*—1/8; *3*—1/9. Equation (2.41), [44]: *4*—Eq. (6.55) at $Re_\omega = 1.0 \times 10^6$; *5*—Eq. (3.27) at σ = 0, n = 1/7 (see Fig. 3.7). Experiments: *6*—$Re_\omega = 0.4 \times 10^6$; *7*—$0.65 \times 10^6$; *8*—$0.94 \times 10^6$; *9*—$1.6 \times 10^6$ [46]; *10*—0.6×10^6; *11*—1.0×10^6 [47]

the viscous sub-layer of the velocity boundary layer; here the radial velocity profile varies linearly depending on the coordinate z (curve 4 in Fig. 6.8). This fact is taken into account in theoretical models [5, 9–11, 32, 42] for large *Pr* and *Sc* numbers.

Next to the wall, the radial velocity v_r varies as a linear function

$$v_r = \frac{\tau_{wr}}{\mu} z = \frac{\tau_w \alpha}{\mu(1+\alpha^2)^{1/2}} z = \frac{\rho V_*^2 \alpha}{\mu(1+\alpha^2)^{1/2}} \frac{c_{\mathrm{f}}}{2} z = \alpha(1+\alpha^2)^{1/2} \omega A_{\mathrm{c}} Re_\omega^{n_{\mathrm{R}}} z. \quad (6.55)$$

Here the constant n_{R} is defined in Eq. (3.31).

The coordinate of the boundary of the viscous sub-layer z_1^+, where the linear model (6.55) holds, can be written as

$$\frac{z_1}{\delta} = \frac{z_1^+}{\gamma(1+\alpha^2)^{1/2} A_{\mathrm{c}}^{1/2} Re_\omega^{1/(1+3n)}}, \quad (6.56)$$

where z_1^+ = 12.54; 13.44; 14.23 and 15.09 for n = 1/7; 1/8; 1/9 and 1/10, respectively (see Chap. 2). According to Eq. (6.56), this corresponds to z_1/δ = 0.01–0.02. Figure 6.8 confirms the validity of the model (6.55) up to $z/\delta_\varphi^{**} = 0.2$, $z/\delta = 0.02$, or $\Delta = \delta_{\mathrm{T}}/\delta = 0.02$.

In the power-law model, the Stanton number is given by Eq. (2.64). In Sect. 2.4.3, the model assumption $\left(z_{1\mathrm{T}}^+/z_1^+\right)^{n_{\mathrm{T}}-1} Pr^{-n_{\mathrm{T}}} = Pr^{-n_{\mathrm{P}}}$ completes Eq. (2.64), whereas validations of this model against experiments deliver the value of the exponent n_{P}.

At high Prandtl or Schmidt numbers, the entire thermal/diffusion boundary layer is included inside the viscous sub-layer of the velocity boundary layer. Hence, one can assume that the relation between the coordinates z_1^+ and $z_{1\mathrm{T}}^+$ (viscous and heat conduction sub-layer) can be recast as

$$(z_{1\mathrm{T}}^+/z_1^+)^{n_{\mathrm{T}}-1} Pr^{-n_{\mathrm{T}}} = K_\alpha Pr^{-n_{\mathrm{P}}}. \quad (6.57)$$

Validations of the model (6.57) against experiments for the *Nu* or *Sh* numbers enable finding the coefficient K_α and exponent n_{P}. Consequently, given $n = n_{\mathrm{T}}$, Eqs. (2.66) and (2.67) turn to

$$St = (c_{\mathrm{f}}/2)\Delta^{-n} Pr^{-n_{\mathrm{P}}} K_\alpha = A_{\mathrm{c}} Re_\omega^{-2n/(3n+1)} \Delta^{-n} Pr^{-n_{\mathrm{P}}} K_\alpha, \quad (6.58)$$

$$Nu = St Re_\omega Pr (1+\alpha^2)^{1/2} = A_{\mathrm{c}} (1+\alpha^2)^{1/2} Re_\omega^{n_{\mathrm{R}}} \Delta^{-n} Pr^{1-n_{\mathrm{P}}} K_\alpha. \quad (6.59)$$

Substituting Eqs. (2.53), (6.55), (6.58) and (6.59) into Eq. (2.20), one can transform the latter to the following notation:

$$\frac{n}{2(n+2)} \alpha\omega \frac{\mathrm{d}}{\mathrm{d}r}\left[r\delta^2 \Delta^2 Re_\omega^{n_{\mathrm{R}}} \Delta T\right] = K_\alpha \Delta^{-n} Pr^{-n_{\mathrm{P}}} Re_\omega^{n_{\mathrm{R}}} \nu \Delta T, \quad (6.60)$$

where Eq. (2.77) determines the boundary layer thickness δ, while $\Delta T = T_w - T_\infty$.

The condition $\Delta = \text{const.}$ is inapplicable to Eq. (6.60), otherwise the exponents at the variable r on the left- and right-hand sides of Eq. (6.60) are not equal to each other.

Let us assume the parameter Δ to be a power-law function

$$\Delta(r) = C_\Delta r^k. \tag{6.61}$$

Substituting Eq. (6.61) into Eq. (6.60) and keeping in mind Eqs. (2.30), (2.77), (2.78) and (3.31), one can finally obtain

$$\Delta = C_{\Delta *} Re_\omega^{k/2}, \tag{6.62}$$

$$C_{\Delta *} = C_{\Delta **} Pr^{-n_\mathrm{p}/(2+n)}, \tag{6.63}$$

$$C_{\Delta **} = \left[\frac{K_\alpha 2(n+2)/n}{\alpha\gamma^2(1 - nk + n_* + 2n_\mathrm{R})}\right]^{1/(n+2)}, \tag{6.64}$$

$$k = -2m/(2+n). \tag{6.65}$$

Equation (6.59) for the Nu number and the expression for Nu_av can be written as follows:

$$Nu = K_1 Re_\omega^{n_{\mathrm{R}*}}, \tag{6.66}$$

$$Nu_\mathrm{av} = K_2 Re_\varphi^{n_{\mathrm{R}*}}, \tag{6.67}$$

$$n_{\mathrm{R}*} = n_\mathrm{R} + mn/(2+n), \tag{6.68}$$

$$K_1 = K_\alpha K_3 C_{\Delta **}^{-n} Pr^{1/3}, \tag{6.69}$$

$$K_2 = 2K_1/(2n_{\mathrm{R}*} + 1), \tag{6.70}$$

$$n_\mathrm{p} = (2+n)/3. \tag{6.71}$$

Equation (6.71) takes into account the fact that the total exponent at the Pr number in Eq. (6.69) must be equal to 1/3.

Thus, in Eqs. (6.66) and (6.67), the total exponent $n_{\mathrm{R}*}$ at the Reynolds number is larger than that in Eq. (3.31) due to the additional term $mn/(2+n)$ (see Eq. (6.68)). This summand emerges as a result of the model with the *variable parameter* Δ being a subsiding function of the coordinate r or, in other words, local Re_ω (see Eq. (6.62)).

The values of the exponent $n_{\mathrm{R}*}$ are: $n_{\mathrm{R}*} = 0.84$ at $n = 1/7$, and $n_{\mathrm{R}*} = 0.868$ at $n = 1/9$. The latter agrees well with the exponent 0.87 at the Re_φ number in the experiment-based Eq. (6.35) [7]. To bring Eq. (8.73) at $n_{\mathrm{R}*} = 0.868$ into agreement with Eq. (6.35), the constant K_α must be equal to $K_\alpha = 1.254$, which yields at $n_* = 0$

$$Nu = 1.52 \times 10^{-2} Re_{\omega}^{0.868} Pr^{1/3}, \quad (6.72)$$

$$Nu_{\text{av}} = 1.11 \times 10^{-2} Re_{\varphi}^{0.868} Pr^{1/3}, \quad (6.73)$$

$$\Delta = 18.31 Re_{\omega}^{-0.3158} Pr^{-1/3}. \quad (6.74)$$

In Fig. 6.7, curve 7 by Eq. (6.73) and curve 3 by Eq. (6.34) merge. Equations (6.72) and (6.35) are also practically identical.

The parameter range in experiments [7] is $Re_{\varphi} = 0.278 \times 10^6$–$1.8 \times 10^6$, $Sc = 930$–$10{,}320$. At minimal values $Sc = 930$ and $Re_{\omega} = 0.278 \times 10^6$ [7], Eq. (6.74) yields $\Delta = 0.036$. Parameter Δ is a decreasing function of the Schmidt and Reynolds numbers. Thus $\Delta = 0.015$ at $Sc = 10{,}320$ and $Re_{\omega} = 0.278 \times 10^6$, whereas $\Delta = 0.02$ at $Sc = 930$ and $Re_{\omega} = 1.8 \times 10^6$. This conforms to the limit $\Delta \leq 0.02$ restricting validity of the linear model of the radial velocity profile.

Model with variable $\boldsymbol{\Delta}$ ***and profile*** $\boldsymbol{T^+}$ ***depending on*** $\boldsymbol{Re_{\omega}}$. In the theoretical works [9–11, 42], the Nusselt number at high *Pr* values is described by a relation

$$Nu = K_{\text{N}}(1 + \alpha^2)^{1/2}(c_{\text{f}}/2)^{1/2} Re_{\omega} Pr^{1/3}, \quad (6.75)$$

where K_{N} is an empirical constant; Eq. (2.82) at $n = 1/7$ was used for $c_{\text{f}}/2$. Local and average Nusselt numbers take a form of Eqs. (6.66) and (6.67), respectively, with

$$K_1 = K_{\text{N}}(1 + \alpha^2)^{1/2} A_{\text{c}}^{1/2} Pr^{1/3}, \quad (6.76)$$

$$n_{\text{R}*} = (2n + 1)/(3n + 1), \quad (6.77)$$

while the constants K_1 and K_2 are related with Eq. (6.70). At $n = 1/7$, Eq. (6.77) brings $n_{\text{R}*} = 0.9$.

Matching Eqs. (6.44) and (6.75) in view of Eq. (6.70), one can obtain $K_{\text{N}} = 0.05986$.

Substitution of Eq. (6.61) into the thermal boundary layer equation yields again Eq. (6.62) for Δ with

$$C_{\Delta *} = C_{\Delta **} Pr^{-1/3}, \quad (6.78)$$

$$C_{\Delta **} = \left[\frac{K_{\text{N}} 2(n + 2)/n}{\alpha \gamma^2 (1 + 2m + 2k + n_* + 2n_{\text{R}}) A_{\text{c}}^{1/2}} \right]^{1/(n+2)}, \quad (6.79)$$

$$k = (2n - 1)/(3n + 1). \quad (6.80)$$

Setting the values $n = 1/7$ and $n_* = 0$ into Eqs. (6.62), (6.78)–(6.80) one can obtain

$$\Delta = 12.54 Re_{\omega}^{-1/4} Pr^{-1/3}. \qquad (6.81)$$

At the lower experimental limit of $Sc = 930$ and $Re_{\omega} = 0.278 \times 10^6$ [7], the value of Δ in view of Eq. (6.81) reduces to $\Delta = 0.037$. For the conditions $Sc = 10{,}320$ and $Re_{\omega} = 0.278 \times 10^6$: $\Delta = 0.016$. For $Sc = 930$ and $Re_{\omega} = 1.8 \times 10^6$: $\Delta = 0.023$. These values for Δ conform to the data obtained by Eq. (6.74) and the upper limiting boundary $\Delta \leq 0.02$ of the validity of the linear model for the radial velocity.

According to the *models with a constant and variable value of* Δ, the function T^+ in wall coordinates, defined by the power-law Eq. (2.23) at $n = n_T$ does not depend on the Reynolds number, which is consistent with the results presented in [48, 49].

Model incorporating Eq. (6.75) results in the profile of T^+ being a function of Re_{ω}

$$T^+ = (z^+)^n (1+\alpha^2)^{-n/2} \gamma^{-n} A_c^{-n/2} C_{\Delta *}^{-n} K_N^{-1} Pr^{2/3} Re_{\omega}^{-0.5(2n^2+n)/(3n+1)}. \qquad (6.82)$$

To conclude, a novel methodology for simulations of temperature/concentration profiles for the values of Pr and Sc much larger than unity was outlined in this section. *An original integral method enabled evaluating a relative thickness Δ of the thermal/diffusion boundary layers that has not been attained by the other investigators. It was demonstrated that the model with a subsiding function Δ(r) yields a new summand in the expression for the exponent at the Reynolds number, which determines functional dependence of* Nu *or* Sh *numbers on the local radius r*. Consequently, theoretical relations obtained for Nusselt and Sherwood numbers are in a good consistency with the selected empirical equations.

References

1. Alden J (1994) Computational electrochemistry. D. Phil. thesis. Chapter 7, Oxford University, Oxford, UK
2. Awad MM (2008) Heat transfer from a rotating disk to fluids for a wide range of Prandtl numbers using the asymptotic model. Trans ASME J Heat Transfer 130(1):014505
3. Barcia OE, Mangiavacchi N, Mattos OR, Pontes J, Tribollet B (2008) Rotating disk flow in electrochemical cells: a coupled solution for hydrodynamic and mass equations. J Electrochem Soc 155(5):D424–D427
4. Daguenet M (1968) Etude du transport de matière en solution, a l'aide des électrodes a disque et a anneau tournants. Int J Heat Mass Transfer 11(11):1581–1596
5. Deslouis C, Tribollet B, Viet L (1980) Local and overall mass transfer rates to a rotating disk in turbulent and transition flows. Electrochim Acta 25(8):1027–1032
6. Dong Q, Santhanagopalan S, White RE (2008) A comparison of numerical solutions for the fluid motion generated by a rotating disk electrode. J Electrochem Soc 155(9):B963–B968
7. Dossenbach O (1976) Simultaneous laminar and turbulent mass transfer at a rotating disk electrode. Berichte der Bunsen-Gesellschaft—Physical Chemistry Chemical Physics 80 (4):341–343
8. Ellison BT, Cornet I (1971) Mass transfer to a rotating disk. J Electrochem Soc 118(1):68–72

9. Kawase Y, De A (1982) Turbulent mass transfer from a rotating disk. Electrochim Acta 27 (10):1469–1473
10. Law CG, Jr, Pierini P, Newman J (1981) Mass transfer to rotating disks and rotating rings in laminar, transition and fully-developed turbulent flow. Int J Heat Mass Transfer 24(5):909–918
11. Levich VG (1962) Physicochemical hydrodynamics. Prentice-Hall Inc, Englewood Cliffs
12. Mohr CM, Newman J (1976) Mass transfer to a rotating disk in transitional flow. J Electrochem Soc 123(11):1687–1691
13. Newman JS (1991) Electrochemical systems, 2nd edn. Prentice-Hall Inc, Englewood Cliffs, New York
14. Şara ON, Erkmen J, Yapici S, Çopur M (2008) Electrochemical mass transfer between an impinging jet and a rotating disk in a confined system. Int Commun Heat Mass Transfer 35 (3):289–298
15. Chen Y-M, Lee W-T, Wu S-J (1998) Heat (mass) transfer between an impinging jet and a rotating disk. Heat Mass Transfer 34(2–3):101–108
16. Cho HH, Rhee DH (2001) Local heat/mass transfer measurement on the effusion plate in impingement/effusion cooling systems. Trans ASME J Turbomach 123(3):601–608
17. Cho HH, Won CH, Ryu GY, Rhee DH (2003) Local heat transfer characteristics in a single rotating disk and co-rotating disks. Microsyst Technol 9(6–7):399–408
18. He Y, Ma LX, Huang S (2005) Convection heat and mass transfer from a disk. Heat Mass Transfer 41(8):766–772
19. Janotková E, Pavelek M (1986) A naphthalene sublimation method for predicting heat transfer from a rotating surface. Strojnícky časopis 37(3):381–393 (in Czech)
20. Koong S-S, Blackshear PL Jr (1965) Experimental measurement of mass transfer from a rotating disk in a uniform stream. Trans ASME J Heat Transfer 85:422–423
21. Kreith F, Taylor JH, Chong JP (1969) Heat and mass transfer from a rotating disk. Trans ASME J Heat Transfer 81:95–105
22. Mabuchi I, Kotake Y, Tanaka T (1972) Studies of convective heat transfer from a rotating disk (6th report, experiment on the laminar mass transfer from a stepwise discontinuous naphthalene disk rotating in a uniformed forced stream). Bull JSME 15(84):766–773
23. Shevchuk IV (2008) A new evaluation method for Nusselt numbers in naphthalene sublimation experiments in rotating-disk systems. Heat Mass Transfer 44(11):1409–1415
24. Shimada R, Naito S, Kumagai S, Takeyama T (1987) Enhancement of heat transfer from a rotating disk using a turbulence promoter. JSME Int J, Ser B 30(267):1423–1429
25. Sparrow EM, Chaboki A (1982) Heat transfer coefficients for a cup-like cavity rotating about its own axis. Int J Heat Mass Transfer 9(25):1334–1341
26. Tien CL, Campbell DT (1963) Heat and mass transfer from rotating cones. J Fluid Mech 17:105–112
27. Wang M, Zeng J (2011) Convective heat transfer of the different texture on the circumferential surface of coupling movement (rotating speed coupling with air velocity) disk. Proc 2011 ICETCE. Lushan, China, pp 1128–1132
28. Wu Y, Wu M, Zhang Y, Wang L (2014) Experimental study of heat and mass transfer of a rolling wheel. Heat Mass Transfer 50(2):151–159
29. Zeng JM, He Y, Wang MH, Ma LX (2011) Analogy study on convection heat transfer on the circumferential surface of rotating disc with naphthalene sublimation. J Qingdao Univ Sci Technol (Natural Sci Ed) 32(5):514–517
30. Shevchuk IV (2009) Convective heat and mass transfer in rotating disk systems. Springer, Berlin
31. Dorfman LA (1963) Hydrodynamic resistance and the heat loss of rotating solids. Oliver and Boyd, Edinburgh
32. Sparrow EM, Gregg JL (1959) Heat transfer from a rotating disc to fluids at any Prandtl number. Trans ASME J Heat Transfer 81:249–251
33. Cheng W-T, Lin H-T (1994) Unsteady and steady mass transfer by laminar forced flow against a rotating disk. Wärme und Stoffübertragung 30(2):101–108

34. Lin H-T, Lin L-K (1987) Heat transfer from a rotating cone or disk to fluids at any Prandtl number. Int Commun Heat Mass Transfer 14(3):323–332
35. Bogdan Z (1982) Cooling of a rotating disk by means of an impinging Jet. Proc 7th IHTC "Heat Transfer 1982". Munich, Germany, vol 3, pp 333–336
36. Elkins CJ, Eaton JK (1997) Heat transfer in the rotating disk boundary layer. Stanford University, Department of Mechanical Engineering, Thermosciences Division Report TSD–103. Stanford University (USA)
37. Popiel CO, Boguslawski L (1975) Local heat-transfer coefficients on the rotating disk in still air. Int J Heat Mass Transfer 18(1):167–170
38. Shevchuk IV (2000) Turbulent heat transfer of rotating disk at constant temperature or density of heat flux to the wall. High Temp 38(3):499–501
39. Shevchuk IV (2005) A new type of the boundary condition allowing analytical solution of the thermal boundary layer equation. Int J Thermal Sci 44(4):374–381
40. Shevchuk IV (2009) An integral method for turbulent heat and mass transfer over a rotating disk for the Prandtl and Schmidt numbers much larger than unity. Heat Mass Transfer 45 (10):1313–1321
41. Wasan DT, Tien CL, Wilke CR (1963) Theoretical correlation of velocity and eddy viscosity for flow close to a pipe wall. AIChE J 9(4):567–569
42. Paterson JA, Greif R (1973) Transport to a rotating disk in turbulent flow at high Prandtl or Schmidt number. Trans ASME J Heat Transfer 95(4):566–568
43. Mishra P, Singh PC (1978) Mass transfer from spinning disks. Chem Eng Sci 33 (11):1449–1461
44. von Karman Th (1921) Über laminare und turbulente Reibung. Z Angew Math Mech 1 (4):233–252
45. Owen JM, Rogers RH (1989) Flow and heat transfer in rotating-disc systems. In: Rotor-stator systems, vol 1. Research Studies Press Ltd., Taunton, Somerset, England
46. Littel HS, Eaton JK (1994) Turbulence characteristics of the boundary layer on a rotating disk. J Fluid Mech 266:175–207
47. Itoh M, Hasegawa I (1994) Turbulent boundary layer on a rotating disk in infinite quiescent fluid. JSME Int J Ser B 37(3):449–456
48. Kader BA (1981) Temperature and concentration profiles in fully turbulent boundary layers. Int J Heat Mass Transfer 24(9):1541–1544
49. Suga K (2007) Computation of high Prandtl number turbulent thermal fields by the analytical wall-function. Int J Heat Mass Transfer 50(25–26):4967–4974